Available online at www.sciencedirect.com
ScienceDirect
Journal of Hazardous Materials 154 (2008) 118–127
Journal of Hazardous Materials
www.elsevier.com/locate/jhazmat

Development of photocatalytic TiO_2 nanofibers by electrospinning and its application to degradation of dye pollutants

Seok Joo Doh*, Cham Kim, Se Geun Lee, Sung Jun Lee, Hoyoung Kim

Advanced Nano Materials Research Team, Daegu Gyeongbuk Institute of Science and Technology (DGIST), Daegu 704-230, South Korea

Received 1 June 2007; received in revised form 28 September 2007; accepted 29 September 2007
Available online 6 October 2007

Abstract

We have developed photocatalytic TiO_2 nanofibers for the treatment of organic pollutants by using electrospinning method. We found that the optimized electrospinning conditions (electric field and flow rate) were 0.9 kV cm^{-1} and 50 μL min^{-1}. After annealing at 550 °C for 30 min, we fabricated TiO_2 nanofibers (average 236 nm thick) with anatase crystalline phase. To increase photocatalytic activity and effective surface area, we coated photocatalytic TiO_2 particles on the TiO_2 nanofibers by using sol–gel method. The degradation rate ($k' = 85.4 \times 10^{-4}$ min^{-1}) of composite TiO_2 was significantly higher than that (15.7×10^{-4} min^{-1}) of TiO_2 nanofibers and that (14.3×10^{-4} min^{-1}) of TiO_2 nanoparticles by the sol–gel method. Therefore, we suggested that the composite TiO_2 of nanofibers and nanoparticles be suitable for the degradation of organic pollutants.

Keywords: TiO_2; Nanofibers; Photocatalytic; Pollutants; Dye; Degradation

1. Introduction

Colored wastewater from textile or dye industries has become a serious environmental problem. Due to the nature of synthetic dyes, conventional biological treatment methods were ineffective for decoloring such dye pollutants [1]. Therefore, chemical and physical methods were combined with biological methods. Physical methods of decolorization include precipitation, adsorption, filtration, and reverse osmosis. Chemical methods of decolorization were reduction, oxidation complexiметric methods, ion exchange and neutralization. However, traditional methods including physical, chemical and biological methods had difficulties in the complete destruction of dye pollutants, and the further disadvantage of secondary pollution [2].

Recently, numerous studies have concentrated on the degradation of toxic organic compounds in wastewater via photocatalysis of various semiconductors [3–17]. Among the photocatalysts, TiO_2 with anatase phase has been most widely investigated due to its acceptable photocatalytic activity and chemical stability, non-environmental effect and low cost [18].

TiO_2 was usually used as powder in solution, which had high photocatalytic efficiency. However, the catalysts should be separated from the purified water after treatment. To solve the problem, a photocatalytic membrane reactor has been developed by using various membrane techniques [19–24]. For a membrane reactor, development of filters and complex apparatus is required and the process cost is relatively high. Meanwhile, the immobilization of TiO_2 catalysts on various substrates has also been studied [25,26]. In case of immobilization, the removal efficiencies of organic pollutants significantly decreased due to the reduction of the photocatalytic active surface area. Therefore, it was very important to develop an immobilized TiO_2 with a high active surface area.

In this paper, we have studied the immobilization of TiO_2 catalysts with high efficiency and high active surface area by utilizing the electrospinning method. Conventionally, the electrospinning method has been used to prepare polymer fibers with diameters ranging from tens of nanometers to submicrometers. Recently, the electrospinning method has also been studied to fabricate one-dimensional inorganic semiconductors such as TiO_2 and ZnO. This is due to their potential applications in environmental remediation and protection, photocatalysis, dye-sensitized solar cells, gas sensors, and batteries [27–35]. In this sense, we have developed photocatalytic TiO_2 nanofibers by electrospinning method for application to the degradation of dye

* Corresponding author. Tel.: +82 53 430 8433; fax: +82 53 430 8443.
E-mail address: sjdoh@dgist.ac.kr (S.J. Doh).

0304-3894/$ – see front matter © 2007 Elsevier B.V. All rights reserved.
doi:10.1016/j.jhazmat.2007.09.118

pollutants. We also coated the photocatalytic TiO_2 particles on the TiO_2 nanofibers to enhance degradation efficiency of dye pollutants. We found that the composite TiO_2 of nanofibers and nanoparticles was suitable for application to the degradation of organic dye pollutants.

2. Materials and methods

2.1. Preparation of TiO_2 nanofibers, TiO_2 films (nanoparticles) and composite TiO_2 (nanofibers and nanoparticles)

Electrospinning is a relatively simple method for fabricating ultrafine fibers with diameters ranging from tens of nanometers to submicrometers [36,37]. The surface of a polymer solution droplet is charged by high voltage to induce the ejection of a liquid jet. The ejected liquid jet is solidified at the collector.

Fig. 1 shows the schematic diagram of electrospinning and picture of a capillary tip. First, we prepared an electrospinning solution which was composed of titanium-tetraisopropoxide (TTIP, 1 g), acetic acid (1 g), polyvinylacetate (PVAc, 1 g) and ethanol (4 ml). The electrospinning solution was placed into a 10 ml syringe with a capillary tip whose inner diameter was 0.5 mm. A copper wire connected to the positive electrode was connected to the polymer solution. A stainless steel plate was used as the collector, which was connected to the ground. We also placed glass substrates (35 mm × 75 mm) on the collector to form TiO_2 nanofibers on the substrate. The electrospinning distance (tip-to-collector distance) was 20 cm. A high voltage power supply (0–35 kV) was employed to generate the electric field. A syringe pump was utilized to control the flow rate of the solution droplet. We varied the voltage and flow rates to optimize the electrospinning conditions.

After fabrication of the precursor nanofibers, we annealed the precursor nanofibers in the box furnace to remove organic substances and to form crystalline TiO_2 nanofibers (the temperature rising rate: 10 °C min^{-1}). We also varied the annealing temperature to investigate the optimum annealing temperature.

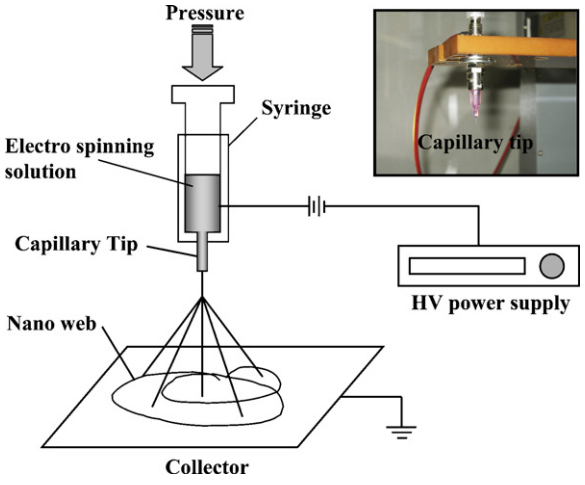

Fig. 1. The schematic diagram of an electrospinning. Inset shows a capillary tip.

The optimization of electrospinning conditions and annealing temperature will be discussed in Section 3 in detail.

To increase photocatalytic activity and effective surface area, we prepared composite TiO_2 by coating photocatalytic TiO_2 nanoparticles on the TiO_2 nanofibers by sol–gel method. The thickness of the composite TiO_2 (nanofibers and nanoparticles) was about 1.3 μm, which was measured by cross-sectional SEM image. For comparison, we also made sol–gel TiO_2 films with nanoparticles on the glass substrate (35 mm × 75 mm).

First, we prepared a 3.5% sol solution by following process. Titanium-tetraisopropoxide (JUNSEI, 98.0% TTIP, 58.6 ml) was added to the ethanol solution (J.T. Baker, 99.9%, 200 ml). To hydrolyze the TTIP, mixture solution was added dropwise to the nitric acid aqueous solution (100 ml, pH 1.5) under vigorous stirring for 1 h. We continued the stirring for further 12 h until a clear solution of TiO_2 nanoparticles was formed. Then, we dipped the glass substrate coated with nanofibers and bare glass substrate in the sol solution. After that, we slowly pulled out the two substrates from the sol solution and dried at 80 °C to obtain solid nanoparticle matrices. We repeated the dipping and drying process five times to complete a thicker coating. After coating the TiO_2 nanoparticles, we annealed the coated samples at 450 °C for 30 min to crystallize the nanoparticles into crystalline phase.

For a practical application, it is needed to have a good adhesion property. To investigate adhesion properties, we performed tape test according to ASTM standards (ASTM D3339). We first cut the surface of each sample in lattice pattern with 1 mm spacing and attached 3M tape. Then, we pulled it off steadily at an angle as close as possible to 60°. As a result, we found that the nanofibers and composite TiO_2 (nanofibers and nanoparticle) had bad adhesion properties (1B classification), though TiO_2 films (nanoparticles) had a good adhesion property (4B classification). We thought that the glass substrate was not compatible with TiO_2 nanofibers. Therefore, some alternative substrates or adhesion technologies should be studied. Fortunately, there was no peeling off of the catalysts during the photocatalytic experiment.

2.2. Photocatalytic experiments

The photocatalytic activities of TiO_2 nanofibers, sol–gel TiO_2 films (nanoparticles) and composite TiO_2 (nanofibers and nanoparticles) were investigated by an analysis of the degradation of dyes under UV illumination. The glasses which were coated by TiO_2 nanofibers, sol–gel TiO_2 nanoparticles and composite TiO_2 were settled in a quartz cell (45 mm × 45 mm × 100 mm) containing dye aqueous solution (10 mg L^{-1}). We used three kinds of dye (C.I: basic blue 26, basic green 4 and basic violet 4). UV irradiation was provided by a 60 W black light bulb (10 W × 6). Prior to photocatalytic reaction, the dye aqueous solution with TiO_2-coated glass was kept in the dark for 60 min to establish an adsorption–desorption equilibrium. The concentration of dye solution was measured with UV irradiation time by using a UV–vis spectrophotometer. The changes in concentration of dye solutions were evaluated from the changes in absorbance at absorption maximum.

2.3. Characterization

The crystalline structure of TiO_2 nanofibers, sol–gel TiO_2 films (nanoparticles) and composite TiO_2 (nanofibers and nanoparticles) were investigated by X-ray diffractometer (XRD, D/Max-2500, Rigaku) using Cu Kα radiation at 40 kV, 100 mA. Surface morphologies and fiber diameters were measured by field-emission scanning electron microscope (S-4800 FE-SEM, Hitachi). The degradation of dye was measured by UV–vis spectrophotometer (Cary 50, Varian). The BET surface area of each sample was measured by surface area and porosity analyzer (ASAP 2020, Micromeritics).

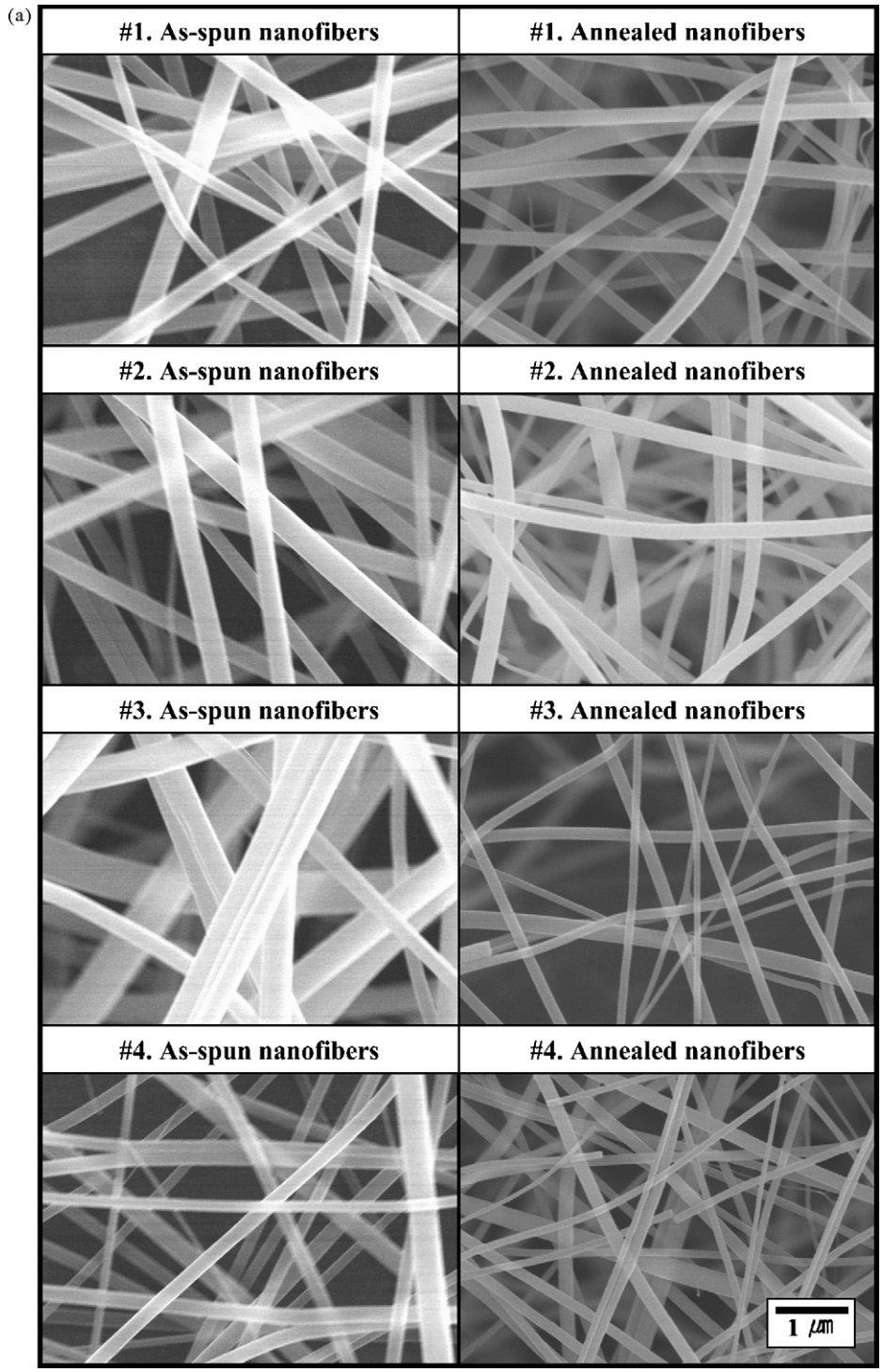

Fig. 2. (a) FE-SEM images of as-spun nanofibers and annealed nanofibers (#1–#4). (b) FE-SEM images of as-spun nanofibers and annealed nanofibers (#5, #6, #8, #9).

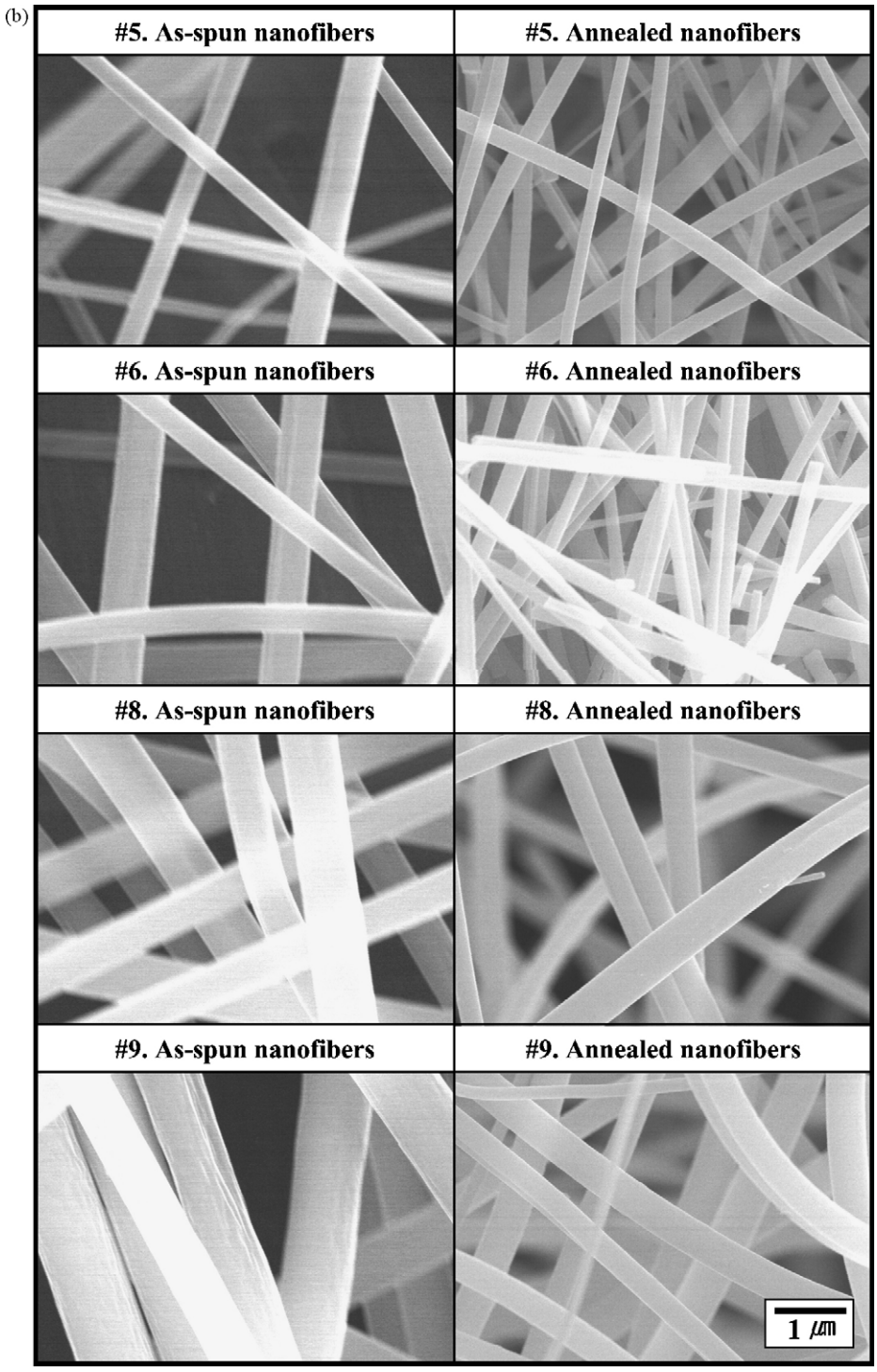

Fig. 2. (*Continued*).

3. Results and discussion

To prepare TiO_2 nanofibers, we investigated the effect of process parameters of electrospinning such as a spinning electric field and solution flow rate. First, we fixed the electrospinning distance as 20 cm. Then, we varied the electric field as 1.2 kV cm^{-1}, 0.9 kV cm^{-1} and 0.5 kV cm^{-1} by changing the electric potential. The solution flow rate was also varied as 20 μL min^{-1}, 50 μL min^{-1} and 100 μL min^{-1} by syringe pump. We summarized the electrospinning conditions, diameter of nanofibers and characteristics of electrospinning in Table 1.

At a high electric field (1.2 kV cm^{-1}), electrospinning processes were discontinuous. That is because the highly charged liquid precursor in the capillary tip was spontaneously ejected to the collector until the syringe pump filled up the capillary tip with a precursor solution. At relatively moderate electric field (0.9 kV cm^{-1}), the electrospinning processes were continuous and stable, regardless of the flow rate. At low electric field

Table 1
Electrospinning condition and fiber diameters of TiO_2 nanofibers

No.	Electric field ($kV\,cm^{-1}$)	Flow rate ($\mu L\,min^{-1}$)	Diameter of nanofibers (as-spun)	Diameter of nanofibers (after annealing)	Characteristics of electrospinning
1	1.2	20	350 ± 68	231 ± 34	Discontinuous
2	1.2	50	322 ± 84	243 ± 70	Discontinuous
3	1.2	100	429 ± 125	168 ± 45	Discontinuous
4	0.9	20	285 ± 123	178 ± 79	Continuous
5	0.9	50	416 ± 100	236 ± 103	Continuous
6	0.9	100	554 ± 150	198 ± 59	Continuous
7	0.5	20	–	–	No deposition
8	0.5	50	695 ± 94	423 ± 104	Continuous, thick fiber
9	0.5	100	874 ± 206	432 ± 143	Continuous, thick fiber

($0.5\,kV\,cm^{-1}$), the electrospinning processes were continuous except low flow rate ($20\,\mu L\,min^{-1}$). From the characteristics of electrospinning with various electric fields, we concluded that a moderate electric field ($0.9\,kV\,cm^{-1}$) was most suitable for the electrospinning of precursor nanofibers of TiO_2.

Fig. 2 shows the FE-SEM images of as-spun nanofibers and annealed nanofibers at 450 °C for 30 min. As shown in the figure, we obtained well-formed nanofibers with diameters ranging from 300 nm to 900 nm. The diameters of nanofibers were dependent on the electric field and flow rate. We also found that the diameter of nanofibers decreased after annealing due to the removal of organic substances in the as-spun nanofibers.

Fig. 3 shows the average diameter of as-spun and annealed nanofibers with the electrospinning parameters. When increasing the electric filed, the average diameter of as-spun nanofibers decreased. With a high electric field, the liquid precursor solution is highly charged and the high electric force overcomes the surface tension of liquid, resulting in a decrease of diameter. By increasing the flow rate for the same electric field, the average diameter of nanofibers increased due to the decrease of the charge in the unit volume of the precursor liquid. As previously mentioned, the diameter of nanofibers decreased after annealing due to the removal of organic substances. The average diameters of the annealed nanofibers ranged from 180 nm to 430 nm and roughly followed the trend of as-spun nanofibers.

We have developed TiO_2 nanofibers for application to the degradation of dye pollutants. Therefore, it is preferable to fabricate thin nanofibers to increase the surface area. In the meantime, we should consider the mass production of nanofibers with continuous and stable process. From the results of characteristics of an analysis of the electrospinning and the diameters with experimental parameters, we concluded that the optimum electric field was $0.9\,kV\,cm^{-1}$ and the optimum flow rate was $50\,\mu L\,min^{-1}$ in this experiment.

To remove the organic substances in the precursor nanofibers and to form crystalline TiO_2 nanofibers, we annealed the as-spun nanofibers at 450 °C for 30 min. However, we did not optimize the annealing temperature and did not confirm whether the annealed nanofibers were crystalline phases. To optimize the annealing temperature of nanofibers, we annealed the as-spun nanofibers ($0.9\,kV\,cm^{-1}$, $50\,\mu L\,min^{-1}$) at various annealing temperatures.

Fig. 4 shows the X-ray diffraction patterns with annealing temperatures. As shown in the figure, there were no diffraction peaks for as-spun (R.T.) and annealed (250 °C) nanofibers,

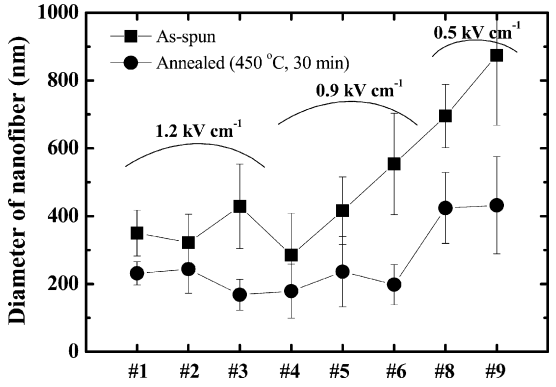

Fig. 3. The average diameter of as-spun and annealed nanofibers with the electrospinning parameters.

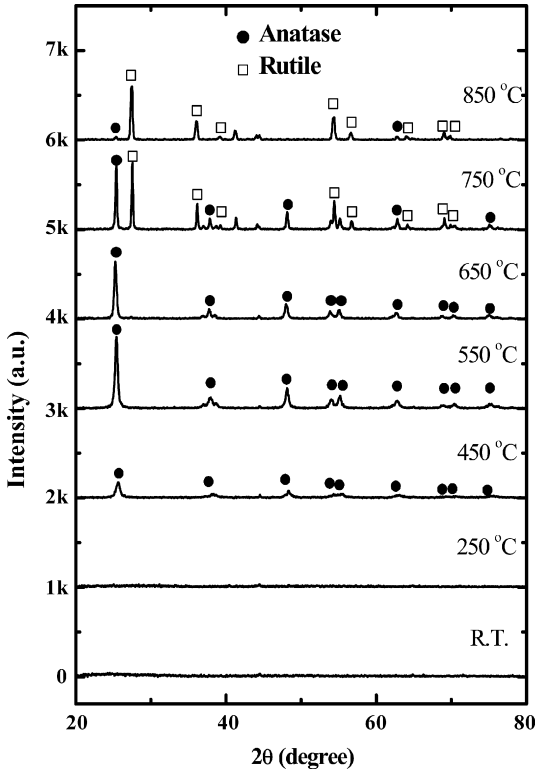

Fig. 4. The X-ray diffraction patterns with annealing temperatures.

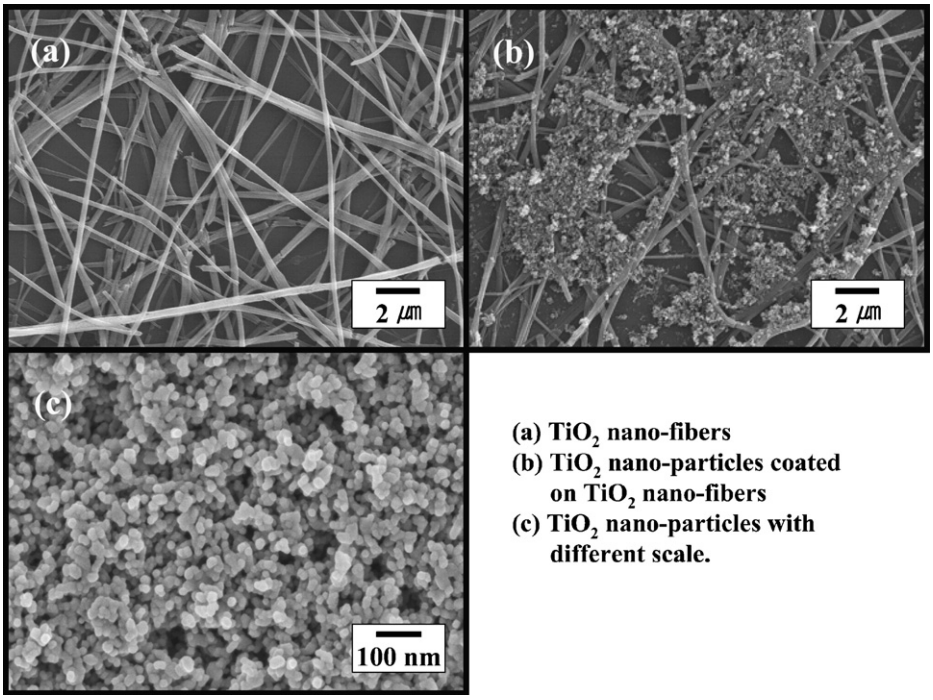

Fig. 5. FE-SEM images of (a) TiO_2 nanofibers, (b) composite TiO_2 (nanofibers and nanoparticles) and (c) TiO_2 nanoparticles with different scale.

which showed the nanofibers were amorphous up to 250 °C. As the annealing temperature increased to 450 °C, the precursor nanofibers started to crystallize into the anatase phase. The diffraction peak was found to be anatase TiO_2 (1 0 1), (0 0 4), (2 0 0), (1 0 5), (2 1 1), (2 0 4), (1 1 6), (2 2 0) and (2 1 5) diffraction peak (anatase TiO_2, JCPDS 21-1272). The multiple diffraction peaks showed that the TiO_2 crystalline phase was a randomly oriented polycrystalline phase. We also found that the average domain size of the crystalline phase was ~17 nm by analyzing FWHM (full width at half maximum) of the diffraction peak and using a Scherrer equation. Therefore, we concluded that the nanofibers (~236 nm) were composed of a polycrystalline anatase TiO_2 phase with a small domain size (~17 nm) and the uncrystallized amorphous phase of a precursor at 450 °C.

As the annealing temperature increased to 550 °C, the intensity of the anatase TiO_2 diffraction peak greatly increased, indicating further crystallization. The domain size of the anatase TiO_2 crystalline phase increased to ~24 nm at 550 °C. With an increase of the annealing temperature further to 750 °C, rutile TiO_2 (1 1 0), (1 0 1), (1 1 1), (2 1 0), (2 1 1), (2 2 0), (3 1 0) and (1 1 2) diffraction peak (rutile TiO_2, JCPDS 21-1276) appeared with an anatase TiO_2 diffraction peak. At 850 °C, the anatase TiO_2 phase almost transformed into a rutile TiO_2 phase. Photocatalytic characteristics of the rutile phase have been known to be inferior to that of the anatase phase. Therefore, we thought that the annealing temperature should be lower than 650 °C. Considering the peak intensity of 550 °C was higher than 650 °C, we concluded that the optimum annealing temperature was 550 °C. We also confirmed that all organic substances were removed after 550 °C for 30 min annealing by Thermogravimetric analysis (data not shown).

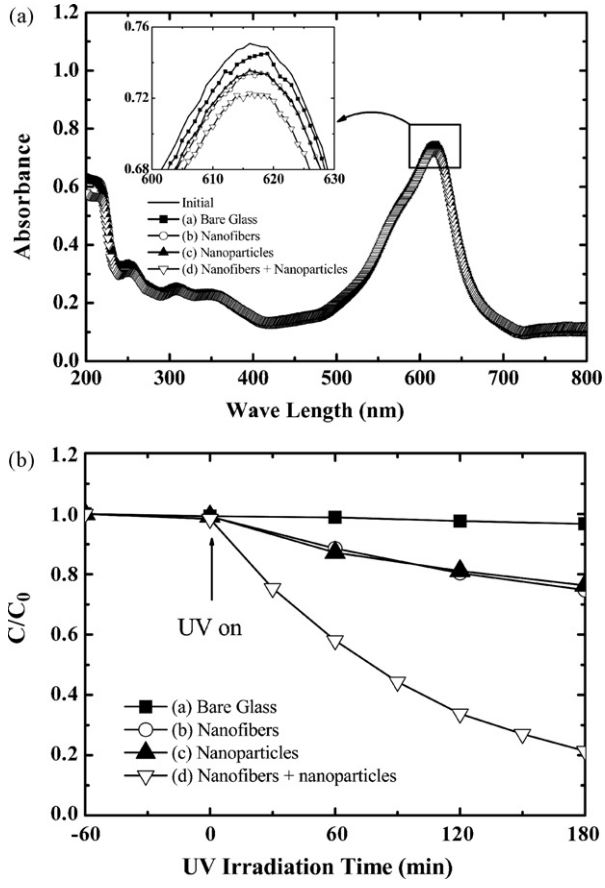

Fig. 6. (a) The initial dye (basic blue 26) adsorption for 1 h without UV irradiation and (b) the photocatalytic degradation of the dye with UV irradiation.

To increase photocatalytic activity and the effective surface area, we prepared composite TiO_2 by coating photocatalytic TiO_2 nanoparticles on the TiO_2 nanofibers with the sol–gel (3.5% sol) method. Fig. 5 shows FE-SEM images of (a) TiO_2 nanofibers (550 °C for 30 min annealing, average 236 nm thick), (b) composite TiO_2 of nanofibers and nanoparticles and (c) TiO_2 nanoparticles with different scale. The average size of the TiO_2 nanoparticles was about 25 nm.

Fig. 6 shows the initial dye adsorption without UV irradiation and photocatalytic degradation of organic dye with UV irradiation. Basic blue 26 was chosen as a model organic pollutant. In this experiment, we investigated adsorption behaviors and photocatalytic activities of TiO_2 nanofibers, sol–gel TiO_2 films (nanoparticles) and composite TiO_2 (nanofibers and nanoparticles). For comparison, a blank experiment with bare glass substrate was also conducted.

Fig. 6(a) shows UV–vis spectra, which were measured after 60 min adsorption on each sample without UV irradiation. As shown in the figure, only small concentration changes were observed due to small adsorption. Inset figure shows the magnified spectra at maximum absorption peak. From the absorption maximum, we calculated the amount of adsorbed dye on the catalyst surface. Bare glass substrate adsorbed 0.9% dye from the initial concentration. TiO_2 nanofibers and sol–gel TiO_2

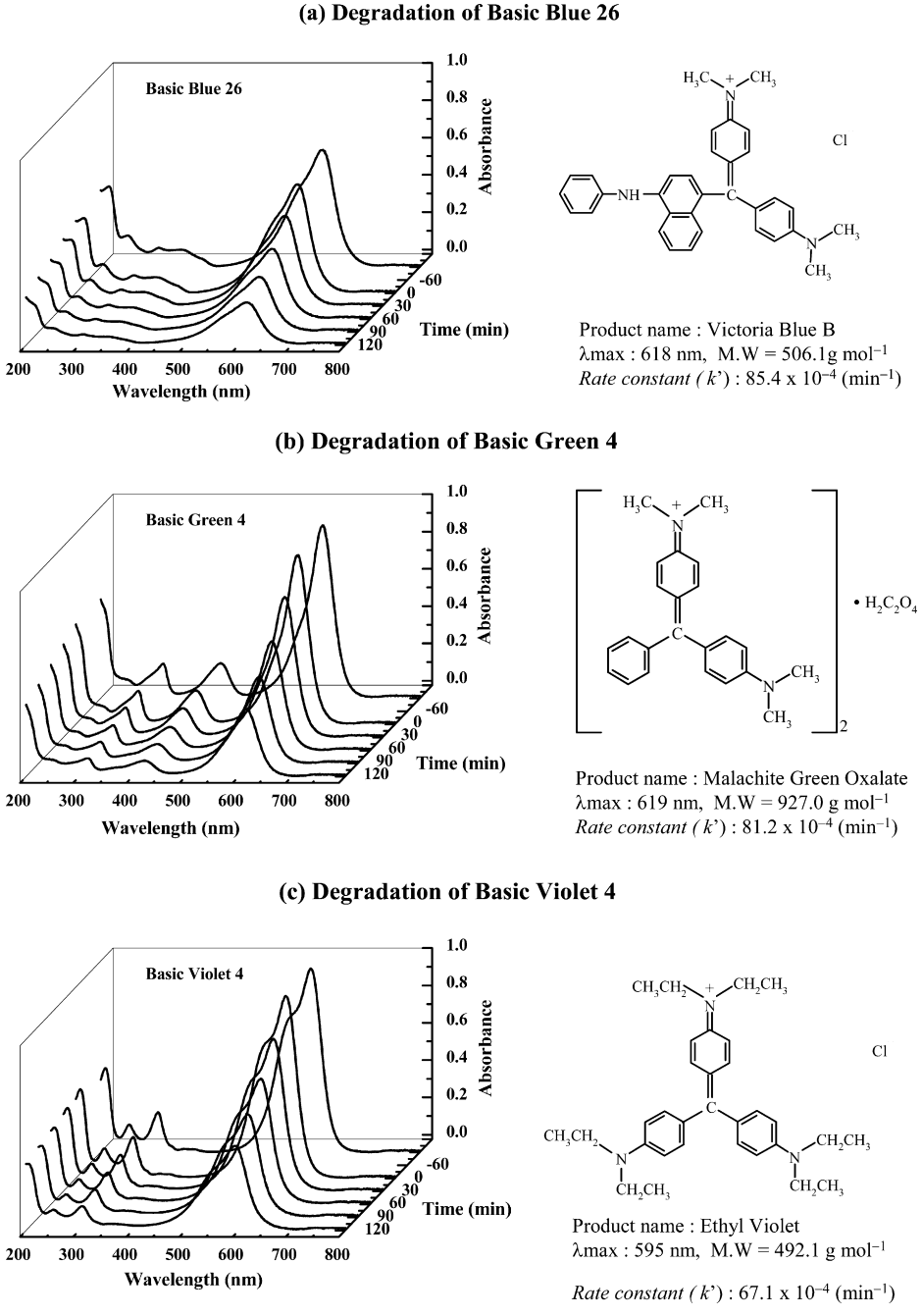

Fig. 7. UV–vis spectral changes of (a) basic blue 26, (b) basic green 4 and (c) basic violet 4 as a function of UV irradiation time.

films (nanoparticles) adsorbed 1.9% and 1.8% dye, respectively. Meanwhile, composite TiO_2 (nanofibers and nanoparticles) adsorbed 3.2% dye, larger than those of nanofibers and nanoparticles.

We attribute the larger adsorption of composite TiO_2 to the complex pore structures, resulting in the large effective surface area. The composite TiO_2 had macro pores between nanofibers and nanopores between nanoparticles. We thought that the dye molecule can first diffuse into macropores in short time and then, finally diffuse into nanopores in long time. Therefore, though composite TiO_2 had smaller BET surface area ($39\,m^2\,g^{-1}$) than that ($50\,m^2\,g^{-1}$) of nanoparticles, the adsorption of the dye on composite TiO_2 was larger than that on nanoparticles in short time (60 min) due to the existence of macropores. Meanwhile, nanofibers also had macropores as composite TiO_2, but the BET surface area ($26\,m^2\,g^{-1}$) of nanofibers was smaller than that ($39\,m^2\,g^{-1}$) of composite TiO_2, resulting in the smaller adsorption.

Fig. 6(b) shows the photocatalytic degradation of the dye with UV irradiation time. The photocatalytic degradation of organic dye is initiated by photoexcitation of the semiconductor, followed by the formation of an electron–hole pair on the surface of catalyst (Eq. (1)). The high oxidative hole directly oxidizes the dye to degrade (Eq. (2)). Very reactive hydroxyl radicals can also be formed either by the decomposition of H_2O (Eq. (3)) or by the reaction of the hole with OH^- (Eq. (4)). The hydroxyl radicals can easily degrade the organic dye (Eq. (5)). The following equations (Eqs. (1)–(5)) summarize the general mechanism of photocatalysis [38,39].

$$TiO_2 + h\nu \rightarrow e^- + h^+ \quad (1)$$

$$h^+ + \text{dye} \rightarrow \text{dye}^{\bullet +} \rightarrow \text{Oxidation of dye} \quad (2)$$

$$h^+ + H_2O \rightarrow H^+ + {}^{\bullet}OH \quad (3)$$

$$h^+ + OH^- \rightarrow {}^{\bullet}OH \quad (4)$$

$${}^{\bullet}OH + \text{dye} \rightarrow \text{Degradation of dye} \quad (5)$$

After 3 h of UV illumination, 25.3% dye was degraded by the TiO_2 nanofibers. The degradation efficiency was comparable with that (23.7%) of nanoparticles coated on the glass substrate. In the case of composite TiO_2, 78.7% dye was degraded after 3 h of illumination. The dye in this experiment was barely degraded under UV illumination without a photocatalyst.

We also calculated the reaction rate constant by using a pseudo-first-order equation (Eq. (6)), a simplified equation of the Langmuir–Hinshelwood kinetic model (Eq. (7)) [40,41].

$$\ln\left(\frac{C_0}{C}\right) = kKt = k't \quad (6)$$

$$r = \frac{dC}{dt} = \frac{kKC}{1 + KC} \quad (7)$$

where r is the rate of the reaction ($mg\,L^{-1}\,min$), C_0 the initial concentration of the dye ($mg\,L^{-1}$), C the concentration of the dye at time t ($mg\,L^{-1}$), t the illumination time, k the reaction rate constant (min^{-1}), and K is the adsorption coefficient ($L\,mg^{-1}$). As a result, we found that the degradation rate ($k' = 85.4 \times 10^{-4}\,min^{-1}$) of composite TiO_2 was significantly higher than that ($15.7 \times 10^{-4}\,min^{-1}$) of TiO_2 nanofibers and that ($14.3 \times 10^{-4}\,min^{-1}$) of TiO_2 nanoparticles. From the results, we found that degradation efficiency was greatly enhanced by compositing nanofibers and nanoparticles. We also concluded that nanofibers were very useful to the degradation of organic dye pollutants.

Fig. 7(a) shows UV–vis spectral changes of the basic blue 26 as a function of UV irradiation time when composite TiO_2 was used. As observed in Fig. 7, the intensity of the 618 nm absorption band due to the chromophore decreased rapidly under UV irradiation. In addition, no new absorption band appeared in the UV–vis region, indicating the break-up of the chromophore. We also performed the photocatalytic degradation of basic green 4 and basic violet 4 by using composite TiO_2 (Fig. 7(b) and (c)). The rate constants for basic green 4 and basic violet 4 were $81.2 \times 10^{-4}\,min^{-1}$ and $67.4 \times 10^{-4}\,min^{-1}$, comparable to that for basic blue 26. From the photocatalytic activity experiment, we concluded that the composite TiO_2 of nanofibers and nanoparticles had high photocatalytic activity, due to its high active surface area.

The re-use of catalysts is very important. In this sense, we performed photocatalytic repeatability test of each catalyst as shown in Fig. 8. The basic blue 26 ($C_0 = 10\,mg\,L^{-1}$) was chosen as a model dye. We first performed the photocatalytic degradation experiment for 3 h under UV irradiation. Then, we refreshed the photocatalytic reactor with the dye solution with the initial concentration and repeated the photocatalytic degradation experiment. As shown in the figure, the photocatalytic activities of the recycled catalysts slightly decreased after several cycles. However, the photocatalytic activities of the recycled catalysts were immediately recovered after annealing at 450 °C for 30 min. Therefore, we suggest that the immobilized photocatalysts be suitable for the application to the degradation of organic dye pollutants.

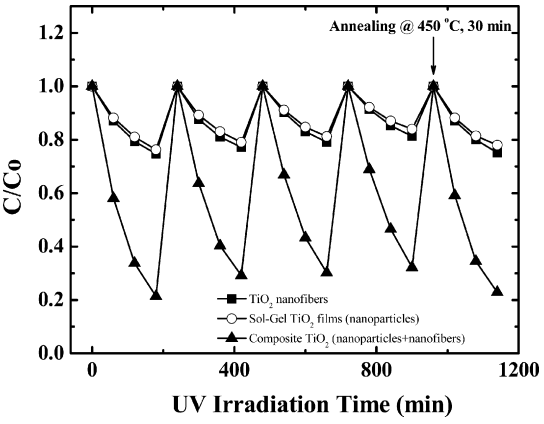

Fig. 8. The photocatalytic repeatability test of TiO_2 nanofibers, TiO_2 nanoparticles and composite TiO_2 (nanofibers and nanoparticles).

4. Conclusions

We have developed the immobilized photocatalytic TiO_2 nanofibers (average 236 nm thick) by using the electrospinning method for application to the degradation of dye pollutants. We found that the optimized electrospinning conditions (electric field and flow rate) and annealing temperature were $0.9\,kV\,cm^{-1}$, $50\,\mu L\,min^{-1}$ and 550 °C. We found that the photocatalytic activity of TiO_2 nanofibers was comparable to that of TiO_2 nanoparticles. We also found that the degradation rate ($k' = 85.4 \times 10^{-4}\,min^{-1}$) of composite TiO_2 was significantly enhanced due to the high effective surface area. We propose that the composite TiO_2 of nanofibers and nanoparticles be suitable for the degradation of organic pollutants.

Acknowledgement

This work was supported by the DGIST Basic Research Program of the Ministry of Science and Technology (MoST) of Korea.

References

[1] I. Arslan, I.A. Balcioglu, Degradation of commercial reactive dyestuffs by heterogeneous and homogenous advanced oxidation processes: a comparative study, Dyes Pigments 43 (2) (1999) 95–108.
[2] F. Herrera, A. Lopez, G. Mascolo, P. Albers, J. Kiwi, Catalytic decomposition of the reactive dye UNIBLUE a on hematite. Modeling of reactive surface, Water Res. 35 (2001) 750–760.
[3] S. Sakthivel, M.V. Shankar, M. Palanichamy, B. Arabindoo, D.W. Bahnemann, V. Murugesan, Enhancement of photocatalytic activity by metal deposition: characterization and photonic efficiency of Pt, Au and deposition on TiO_2 catalyst, Water Res. 38 (2004) 3001–3008.
[4] A.A. Khodja, T. Sehili, J.-F. Pilichowski, P. Boule, Photocatalystic degradation of 2-phenylphenol on TiO_2 and ZnO in aqueous suspensions, J. Photochem. Photobiol. A 141 (2001) 231–239.
[5] M. Mrowetz, E. Selli, Photocatalystic degradation of formic and benzoic acids and hydrogen peroxide evaluation in TiO_2 and ZnO water suspensions, J. Photochem. Photobiol. A 180 (2006) 15–22.
[6] C.A.K. Gouvêa, F. Wypych, S.G. Moraes, N. Durán, N. Nagata, P. Peralta-Zamora, Semiconductor-assisted photocatalystic degradation of reactive dyes in aqueous solution, Chemosphere 40 (2000) 433–440.
[7] A.A. Ismail, I.A. Ibrahim, M.S. Ahmed, R.M. Mohamed, H. El-Shall, Sol–gel synthesis of titania–silica photocatalyst for cyanide photodegradation, J. Photochem. Photobiol. A 163 (2004) 445–451.
[8] X.Z. Li, H. Liu, L.F. Cheng, H.J. Tong, Photocatalystic oxidation using a new catalyst-TiO_2 microsphere-for water and wastewater treatment, Environ. Sci. Technol. 37 (2003) 3989–3994.
[9] Q.X. Dai, H.Y. Xiao, W.S. Li, Y.Q. Na, X.P. Zhou, Photodegradation catalyst discovery by high-throughput experiment, J. Comb. Chem. 7 (2005) 539–545.
[10] C. Chen, W. Zhao, J. Li, J. Zhao, H. Hidaka, N. Serpone, Formation and identification of intermediate in the visible-light-assisted photodegradation of sulforhodamine-B dye in aqueous TiO_2 dispersion, Environ. Sci. Technol. 36 (2002) 3604–3611.
[11] S.O. Obare, T. Ito, M.H. Balfour, G.J. Meyer, Ferrous hemin oxidation by organic halides at nanocrystalline TiO_2 interfaces obare, Nano Lett. 3 (2003) 1151–1153.
[12] A.Y. Nosaka, T. Fujiwara, H. Yagi, H. Akutsu, Y. Nosaka, Photocatalystic reaction site at the TiO_2 surface as studied by solid-state ^{1}H-NMR spectroscopy, Langmuir 19 (2003) 1935–1937.
[13] S. Lee, C. Fan, T. Wu, S.L. Anderson, CO oxidation on Au_n/TiO_2 catalysts produced by size-selected cluster deposition, J. Am. Chem. Soc. 126 (2004) 5682–5683.
[14] J.J. Sene, W.A. Zeltner, M.A. Anderson, Fundamental photoelectrocatalystic and electrophoretic mobility studied of TiO_2 and V-doped TiO_2 thin-film electrode materials, J. Phys. Chem. B 107 (2003) 1597–1603.
[15] H. Park, W. Choi, Photoelectrochemical investigation on electron transfer mediating behaviors of polyoxometalate in UV-illuminated suspensions of TiO_2 and Pt/TiO_2, J. Phys. Chem. B 107 (2003) 3885–3890.
[16] H.G. Kim, D.W. Hwang, J.S. Lee, An undoped, single-phase oxide photocatalyst working under visible light, J. Am. Chem. Soc. 126 (2004) 8912–8913.
[17] C. Burda, Y. Lou, X. Chen, A.C.S. Samia, J. Stout, J.L. Gole, Enhanced nitrogen doping in TiO_2 nanoparticles, Nano Lett. 3 (2003) 1049–1051.
[18] W. Xi, S.-U. Geissen, Separation of titanium dioxide from photocatalytically treated water by cross-flow microfiltration, Water Res. 35 (2001) 1256–1262.
[19] R. Molinari, M. Borgese, E. Drioli, L. Palmisano, M. Schiavello, Hybrid processes coupling photocatalysis and membranes for degradation of organic pollutants in water, Catal. Today 75 (2002) 77–85.
[20] R. Molinari, L. Palmisano, E. Drioli, M. Schiavello, Studies on various reactor configurations for coupling photocatalysis and membrane processes in water purification, J. Membr. Sci. 206 (2002) 399–415.
[21] K. Sopajaree, S.A. Qasim, S. Basak, K. Rajeshwar, An integrated flow reactor-membrane filtration system for heterogeneous photocatalysis. Part I: experiments and modelling of a batch-recirculated photoreactor, J. Appl. Electrochem. 29 (1999) 533–539.
[22] K. Sopajaree, S.A. Qasim, S. Basak, K. Rajeshwar, An integrated flow reactor-membrane filtration system for heterogeneous photocatalysis. Part II: experiments on the ultrafiltration unit and combined operation, J. Appl. Electrochem. 29 (1999) 1111–1118.
[23] R. Molinari, M. Mungari, E. Drioli, A. Di Paola, V. Loddo, L. Palmisano, M. Schiavello, Study on a photocatalytic membrane reactor for water purification, Catal. Today 55 (2000) 71–78.
[24] R. Molinari, C. Grande, E. Drioli, L. Palmisano, M. Schiavello, Photocatalytic membrane reactors for degradation of organic pollutants in water, Catal. Today 67 (2001) 273–279.
[25] M.F.J. Dijkstra, H. Buwalda, A.W.F. de Jong, A. Michorius, J.G.M.A.A.C.M. Winkelman, Beenackers, experimental comparison of three reactor designs for photocatalytic water purification, Chem. Eng. Sci. 56 (2001) 547–555.
[26] I. Sopyan, M. Watanabe, S. Murasawa, K. Hashimoto, A. Fujishima, An efficient TiO_2 thin-film photocatalyst: photocatalytic properties in gas-phase acetaldehyde degradation, J. Photochem. Photobiol. A 98 (1996) 79–86.
[27] H. Guan, C. Shao, S. Wen, B. Chen, J. Gong, X. Yang, A novel method for preparing Co_3O_4 nanofibers by using electrospun PVA/cobalt acetate composite fibers as precursor, Mater. Chem. Phys. 82 (2003) 1002–1006.
[28] P. Viswanathamurthi, N. Bhattarai, H.Y. Kim, D.R. Lee, Vanadium pentoxide nanofibers by electrospinning, Scripta Mater. 49 (2003) 577–581.
[29] X. Yang, C. Shao, H. Guan, X. Li, J. Gong, Preparation and characterization of ZnO nanofibers by using electrospun PVA/zinc acetate composite fiber as precursor, Inorg. Chem. Commun. 7 (2004) 176–178.
[30] N. Dharmaraj, H.C. Park, C.K. Kim, H.Y. Kim, D.R. Lee, Nickel titanate nanofibers by electrospinning, Mater. Chem. Phys. 87 (2004) 5–9.
[31] C. Shao, H. Guan, Y. Liu, X. Li, X. Yang, Preparation of Mn_2O_3 and Mn_3O_4 nanofibers via an electrospinning technique, J. Solid State Chem. 177 (2004) 2628–2631.
[32] G. Zhang, W. Kataphinan, R. Teye-Mensah, P. Katta, L. Khatri, E.A. Evans, G.G. Chase, R.D. Ramsier, D.H. Reneker, Electrospun nanofibers for potential space-based applications, Mater. Sci. Eng. B 116 (2005) 353–358.
[33] V. Tomer, R. Teye-Mensah, J.C. Tokash, N. Stojilovic, W. Kataphinan, E.A. Evans, G.G. Chase, R.D. Ramsier, D.J. Smith, D.H. Reneker, Selective emitters for thermophotovoltaics: erbia-modified electrospun titania nanofibers, Sol. Energ. Mater. Sol. C 85 (2005) 477–488.
[34] S.-H. Lee, C. Tekmen, W.M. Sigmund, Three-point bending of electrospun TiO_2 nanofibers, Mater. Sci. Eng. A 398 (2005) 77–81.
[35] X. Yang, C. Shao, Y. Liu, R. Mu, H. Guan, Nanofibers of CeO_2 via an electrospinning technique, Thin Solid Films 478 (2005) 228–231.

[36] Z.M. Huang, Y.Z. Zhang, M. Kotaki, S. Ramakrishna, A review on polymer nanofibers by electrospinning and their applications in nanocomposites, Compos. Sci. Technol. 63 (2003) 2223–2253.
[37] D. Li, Y. Xia, Electrospinning of nanofibers: reinventing the wheel? Adv. Mater. 16 (2004) 1151–1170.
[38] N. Daneshvar, D. Salari, A.R. Khataee, Photocatalytic degradation of azo dye acid red 14 in water on ZnO as an alternative catalyst to TiO_2, J. Photochem. Photobiol. A 162 (2004) 317–322.
[39] M.H. Habibi, A. Hassanzadeh, S. Mahdavi, The effect of operational parameters on the photocatalytic degradation of three textile azo dyes in aqueous TiO_2 suspensions, J. Photochem. Photobiol. A 172 (2005) 89–96.
[40] A.L. Pruden, D.F. Ollis, Photoassisted heterogeneous catalysis: the degradation of trichloroethylene in water, J. Catal. 82 (1983) 404–417.
[41] D.F. Ollis, Contaminant degradation in water, Environ. Sci. Technol. 19 (1985) 480–484.